

New Integrated Navigation Scheme for the Level 4 Autonomous Vehicles in Dense Urban Areas

Li-Ta Hsu* and Weisong Wen
The Hong Kong Polytechnic University
Kowloon, Hong Kong
Correspondence: lt.hsu@polyu.edu.hk

Abstract—Accurate and globally referenced positioning is fatal to the safety-critical autonomous driving vehicles (ADV). Multi-sensor integration is becoming ubiquitous for ADV to guarantee the robustness and accuracy of the navigation system. Unfortunately, the existing sensor integration systems are still heavily challenged in urban canyons, such as Tokyo and Hong Kong. The main reason behind the performance degradation is due to the varying environmental conditions, such as tall buildings and surrounded dynamic objects. GNSS receiver is an indispensable sensor for ADV, which relies heavily on the environmental conditions. The performance of GNSS can be significantly affected by signal reflections and blockages from buildings or dynamic objects. With the enhanced capability of perception, fully or partially sensing the environment real-time becomes possible using onboard sensors, such as camera or LiDAR. Inspired by the fascinating progress in perception, this paper proposes a new integrated navigation scheme, the perception aided sensor integrated navigation (PASIN). Instead of directly integrating the sensor measurements from diverse sensors, the PASIN leverages the onboard and real-time perception to assist the single measurement, such as GNSS positioning, before it is integrated with other sensors including inertial navigation systems (INS). This paper reviews several PASIN, especially on the GNSS positioning. As an example, GNSS is aided by the perception of a camera or LiDAR sensors, are conducted in dense urban canyons to validate this novel sensor integration scheme. The proposed PASINS can also be extended to LiDAR- or visual- centered navigation system in the future.

Keywords—Autonomous Driving Vehicle; Positioning, Perception, GNSS, LiDAR; Camera, PASIN, Urban canyon

I. INTRODUCTION

The level 4 (L4) autonomous driving vehicles (ADV) [1] are well believed to be the remedy for the excessive traffic accidents and congestions in megacities, such as Hong Kong and Tokyo. To achieve this, robust and globally referenced positioning is required. The multi-sensor fusion [2] is the promising solution which integrates the information from global navigation satellite systems (GNSS) [3], the inertial navigation system (INS), light detection and ranging (LiDAR) and high-definition map (HD Map). The GNSS/INS/LiDAR/HD map [2] integration can obtain decent performance in constrained environments. Unfortunately, its positioning performance can be significantly degraded in challenging environments such as urban canyons [4] with high-rising buildings and numerous dynamic objects [5-8]. The GNSS positioning can be degraded in urban canyons [9-11] due to

the signal blockage and reflections from buildings. The LiDAR-based positioning can be significantly confused due to the excessive dynamic objects [12, 13]. To solve these problems, the straightforward method is to make use of the tactical-grade environmentally independent sensors, the INS, to enhance the resilience against environmental changes. However, the high-cost is, in fact, the key factor which prevents the arrival of autonomous driving vehicles. Instead of depending on expensive sensors, the main researches to solve these problems can be divided into two groups; (1) developing a more robust sensor fusion scheme and (2) developing robust sensor measurement models that are robust to deal with the outlier measurements.

The Kalman filter (KF) and its variants, such as extended KF (EKF), [14] have dominated the multi-sensor fusion for several decades, due to its efficiency and maturity in engineering application. However, one of the major drawbacks is that it fails to make use of historical information [6, 15, 16], due to the first-order Markov assumption [17]. As a result, the state estimation based on filtering can easily be distorted by unmodeled outlier measurements [6]. To solve this problem, the factor graph optimization (FGO) [18] is studied to fuse information from multi-sensors using an optimization scheme. Different from the conventional EKF, the FGO optimize a full state set by considering all the historical information. Numerous scholarly work in the robotics field [19-21] and navigation filed [6, 15, 22] shows the outperforming advantages of FGO, compared with the EKF. The results show that the FGO has stronger resilience against outlier measurements during the sensor fusion. According to our recent findings in [15], this is mainly caused by three parts; (1) the batch data considered during the optimization, (2) the multiple iterations in FGO and (3) the re-linearization in FGO which can effectively reduce the accuracy loss from expanding the 1st order Taylor series from the inaccurate guess in EKF. However, the improvement can still be limited when the healthy measurements are not redundant enough and the sensor measurements noise is not effectively modeled [23, 24].

The other active research stream [23, 25, 26] proposes to develop robust sensor models to mitigate the effects of outlier measurements above the FGO. The switchable constraint algorithm is proposed in [23] where a novel constraint is employed to estimate the possibility of a measurement belonging to an outlier. Significantly improved performance can be obtained on condition that sufficient healthy measurements are available during the FGO. Unfortunately,

this requirement is not always satisfied, such as the GNSS positioning in urban canyons where the polluted signals stands for the majority of all the measurements [6]. The dynamic covariance estimation (DCE) algorithm is proposed in [24] where the covariance of the sensor measurement is estimated simultaneously during the FGO. Improved performance is obtained due to the de-weighting of outlier measurements. However, the DCE relies on the residual of the measurements and the initial guess of the covariance. Different from the conventional Gaussian noise based sensor model, the Gaussian mixture model (GMM) is proposed in [25, 27] in which the sensor noise is modeled using multiple Gaussian components with different weightings. Significantly improved performance is obtained in GNSS and the encoder-based odometer integration using FGO. Unfortunately, the estimation of the parameters for GMM relies heavily on the initial guess of the states. In other words, if the initial guess of the state encodes large error which is typical in urban canyons, the GMM can even distort the FGO.

In short, both the FGO and the robust sensor can help to mitigate the impacts of outlier measurements. However, the improvements can be limited in challenging environments, where the healthy measurements are limited. Since the majority of the outlier measurements are caused by the environment change, therefore, sensing the environment can be a promising approach to identify the outlier measurements. With the fast and fascinating progress of perception based on camera or 3D LiDAR sensors in ADV, partially or fully percept the environment becomes possible. Instead of directly integrating the measurements from diverse sensors using FGO or EKF, this paper proposes a new integrated navigation scheme, the perception aided sensor integrated navigation (PASIN). The PASIN makes use of the onboard and real-time perception capability to rectify the single measurement, such as GNSS positioning, before it is integrated with other sensors, such as INS. The environment surrounding the ego-vehicle is firstly partially or fully perceived based on onboard sensors, such as the camera and/or 3D LiDAR. Then, the quality of the measurement is validated based on the description of the perceived environment. Then, the affected measurements, such as GNSS NLOS signals, are rectified by a novel correction or re-modeling process. Finally, the calibrated measurements are integrated with the other sensors. In fact, the proposed PASIN are verified that it can be applied to diverse sensors in the previous researches, for example, 1) the degradation of LiDAR positioning caused by dynamic objects can be improved by detecting the dynamic objects based on 3D LiDAR [12] or camera [28]; 2) the degradation of GNSS positioning caused by the signal blockage and reflection can be improved by precepting the dynamic objects [7, 29] or surrounding buildings [10, 30] using 3D LiDAR. As the GNSS is one of the indispensable sources which provides globally referenced positioning for ADV and relies heavily on the environment conditions, the rest of this paper focuses on demonstrating the feasibility of the PASIN in improving the GNSS positioning in urban canyons based on the review of our previous researches.

The remainder of this paper is structured as follows. An overview of the proposed PASIN scheme is given in Section

II. Section III presents a LiDAR perception aided GNSS positioning and corresponding experimental validation is also given. The camera/LiDAR aided GNSS positioning is presented in Section IV. Finally, the conclusions and future work are drawn in Section V.

II. OVERVIEW OF THE PROPOSED PASIN SCHEME

The concept of a typical PASIN is illustrated in Fig. 1 where the GNSS positioning is assisted by the perception based on the additional sensors, such as the 3D LiDAR and camera. The inputs of the system include the raw measurements from GNSS receiver, INS, LiDAR and camera. The conventional sensor fusion scheme directly fuses all the measurements using an FGO or EKF estimator. Differently, a novel GNSS measurement correction/re-modeling process is performed before the sensor integration in PASIN. During the correction/re-modeling process, the GNSS quality is validated based on the perceived environment description. Then, the affected GNSS measurement is corrected or re-modeled based on the environment description. Finally, the calibrated measurements are coupled with other sensors either in a tightly or loosely fashions.

The major contributions of this paper are listed as follows:

(1) This paper proposes a new sensor integration scheme, the PASIN which leverages the perceived environment to validate and calibrate the sensor measurements.

(2) This paper demonstrates several applications where GNSS positioning is improved with the help of online perception.

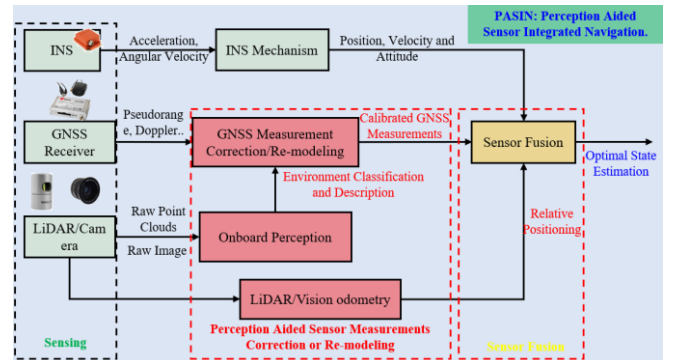


Fig. 1. Illustration of the proposed PASIN, where the GNSS is assisted by the camera or LiDAR-based perception.

III. LiDAR PERCEPTION AIDED GNSS POSITIONING

This section presents the applications of PASIN where the GNSS positioning is assisted by the LiDAR-based perception. Firstly, GNSS NLOS exclusion caused by the dynamic objects is presented in Section III-A based on our previous work in [29]. Secondly, the NLOS correction aided by LiDAR perception and building heights is presented in Section III-B based on our previous work in [10]. Instead of NLOS exclusion or correction (not always applicable due to the difficulty in detecting the reflecting point of NLOS signal [10]), a more general solution, where the NLOS is remodeled during the sensor integration, is presented in Section III-C. The listed three applications, where not all the sensors (camera

and 3D LiDAR) are employed to perceive the environment, are part of the PASIN shown in Fig. 1.

A. GNSS Positioning with NLOS Exclusion Aided by Object Detection

(1) Methodology

In this section, we focus on the NLOS reception caused by the double-decker bus, a representative moving object in Hong Kong. The double-decker bus, that its height is about 4.5 meters, can block signals transmitted from the satellites. Meanwhile, this GNSS signal can be reflected by nearby buildings and finally received by GNSS receiver equipped on top of an autonomous vehicle resulting in NLOS reception. This magnitude of pseudorange error of this NLOS is subjected to the distance from the GNSS receiver to the reflector and the elevation angle of the satellite [9].

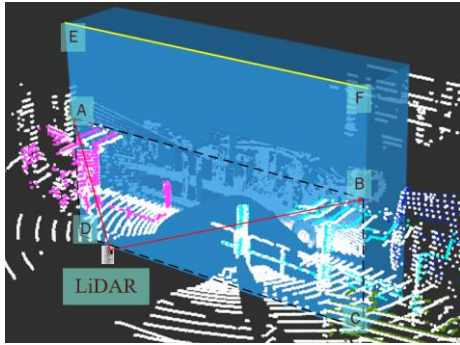


Fig. 2. Illustration of the double-decker bus detection using Euclidean cluster algorithm and parameters-based classification. Blue box ABCD represents the initially detected double-decker bus. Blue box ABFE represents the extended detected double-decker bus. [29].

As an essential sensor for positioning and perception of autonomous driving, 3D LiDAR is installed on the top of the vehicle. In this section, LiDAR is employed to detect the surrounding double-decker buses as shown in Fig. 2. Then, NLOS exclusion is implemented based on detected double-decker boundary parameters which are projected into a skyplot, which described the distribution of satellites in terms of elevation and azimuth angles [31]. Finally, GNSS WLS positioning is conducted using the remaining satellites. Fig. 3 shows the flowchart of the proposed algorithm: improved GNSS positioning by NLOS exclusion based on object detection of LiDAR point cloud. The inputs of the chart include two parts, raw measurements and satellite information from GNSS and 3D point cloud by LiDAR. Moreover, the yaw angle from INS is also an input for coordinate transformation. The output is the GNSS positioning result. The proposed method can be executed as follows:

Step I: Euclidean clustering is employed to transfer real-time 3D point clouds into several clusters, as known as the point cloud segmentation. The parameters-based classification method is utilized to classify the clusters and identify the double-decker bus from multi-clusters.

Step II: Satellites and the double-decker bus are projected into a skyplot based on their azimuth and elevation angles relative to the GNSS receiver.

Step III: Considering satellite elevation, azimuth angles, SNR and double-decker bus boundary information (elevation and azimuth angles in skyplot), satellites that blocked by double-decker bus are excluded.

Step IV: Implementing GNSS WLS positioning using the surviving satellites after the NLOS exclusion by Step III.

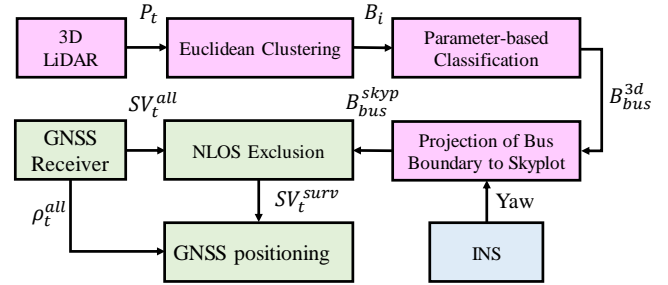


Fig. 3. Overview of the proposed algorithm of NLOS exclusion and GNSS positioning flowchart [29]. Inputs are the 3D point cloud from 3D LiDAR, yaw angle from INS and raw measurements from GNSS receiver. The output is the GNSS positioning result based on the surviving satellites after NLOS exclusion.

(2) Experimental Evaluation

The dynamic experiment is implemented in an urban area of Hong Kong to demonstrate the effectiveness of the proposed method. We use the GNSS-RTK/INS integrated system (NovAtel SPAN-CPT) to provide the reference trajectory of the experiment. This device is commonly used for ground truth of positioning among academic fields and industry fields. The u-blox M8T receiver is used to collect raw GPS and BeiDou raw measurements. 3D LiDAR sensor, Velodyne 32, is employed to provide the real-time point cloud. To verify the effectiveness of the proposed method, four methods were compared, the “EF” represents the “elevation filter”. This means that the elevation angle threshold is applied, where the satellite with an elevation angle less than ele_{thres} is excluded from the further WLS.

- (1). LS positioning (LS)
- (2). LS positioning + ele_{thres} (LS-EF)
- (3). WLS positioning + ele_{thres} (WLS-EF)
- (4). WLS positioning + ele_{thres} + NLOS exclusion (WLS-EF-NE)

The skyplot representing one epoch in the test can be seen in Fig. 4. Satellite 6, 30 and 88, with elevations of 41° , 23° , and 46° respectively, are excluded, due to the blockage from the double-decker bus. There are still about 12 satellites including GPS and BeiDou remained which are sufficient for the GNSS positioning.

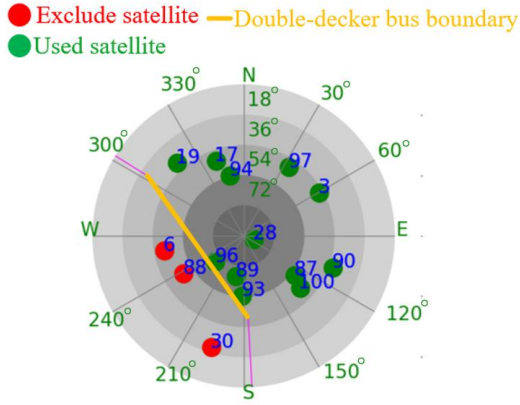


Fig. 4. A skyplot snapshot indicating the satellite distribution during the dynamic experiment. The green circle represents the satellites that are healthy, which will be used in GNSS positioning. The red circle denotes the excluded satellites. The yellow line indicates the edge boundary of a double-decker bus [29].

TABLE I. POSITIONING PERFORMANCE OF THE FOUR METHODS IN THE DYNAMIC TEST (IN THE UNIT OF THE METER) [29]

All data	LS	LS-EF	WLS-EF	WLS-EF-NE
MAE	47.59m	44.98m	13.19m	5.04m
Std	42.07m	40.99m	14.67m	2.87m
RMSE	58.61m	52.17m	16.58m	6.29m
Percentage (MAE<5 meters)	29.71%	30.23%	46.51%	53.49%
Percentage (MAE<10 meters)	37.16%	41.86%	60.47%	95.35%
Percentage (MAE>15 meters)	60.35%	55.81%	30.23%	0%

TABLE I shows the GNSS positioning performance using four positioning methods. With the proposed method, decent improvements are obtained. Firstly, the positioning error declines from 13.19 meters to 5.04 meters in the tested dynamic experiment, which obtains about 61.79 % of the improvements, compared with the WLS-EF method. The standard deviation drops from 14.67 to 2.87 meters. Interestingly, 53.49 % of the results have a MAE of less than 5 meters and approximately 95.35 % of the results possess errors less than 10 meters. Both GNSS positioning accuracy and standard deviation are improved using the proposed method.

B. GNSS Positioning with NLOS Correction Aided by Object Detection

(1) Methodology

Fully NLOS exclusion can, in fact, significantly distort the geometry distribution of satellites which is not acceptable in deep urban canyons [10]. Instead of directly performing NLOS exclusion, this section explores the feasibility of correcting the NLOS measurements caused by surrounding buildings with the aid of 3D LiDAR-based perception. Fig. 5 presents direct propagation routes, multipath and potential NLOS receptions of GNSS signals. The buildings, of which height is indicated by H , can block a signal transmitted from

a satellite, for example, satellite 1 in Fig. 5. Meanwhile, this GNSS signal is reflected by the other nearby building and finally received by the GNSS receiver equipped on top of the autonomous vehicle, which results in NLOS receptions. Actually, this scenario is a regular case in Hong Kong. The number of satellites visible to the GNSS receiver is related to the height of buildings and the distance from the receiver to the building, which is denoted as α in Fig. 5.

In this section, LiDAR is employed to detect the surrounding building surfaces and obtain the distance from the GNSS receiver to the building surface, and then the top edges of buildings (TEBs) can be identified consequently. Then, NLOS detection and correction is implemented based on detected TEBs, which are projected into a skyplot, and the distance from GNSS receiver to buildings. Finally, GNSS positioning is performed using both the corrected and healthy pseudorange measurements. Fig. 6 shows the flowchart of the proposed method. The proposed method can be executed as follows:

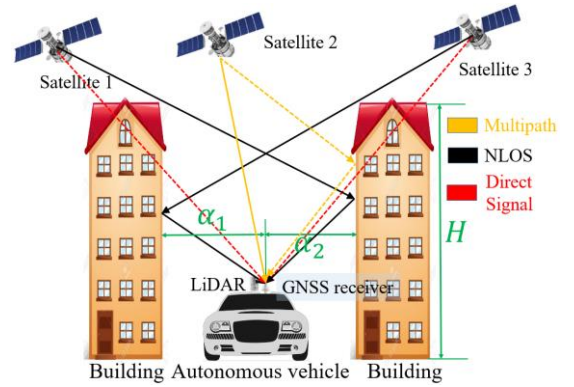


Fig. 5. Illustration of GNSS signal transmission routes in the urbanized area in Hong Kong. NLOS/multipath can be caused by surrounding buildings [10].

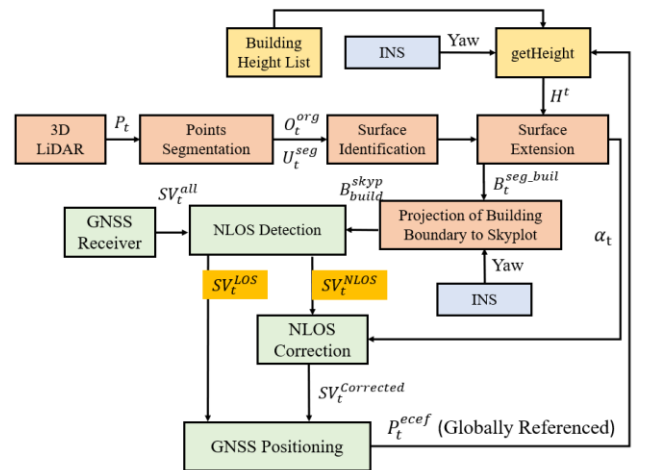


Fig. 6. Flowchart of the proposed method of GNSS SPP with NLOS correction. The inputs are the 3D LiDAR, INS, building height list, and GNSS raw measurements [10].

Step I: The point cloud segmentation method is employed to detect the building surface. The geometry dimensions and pose of the detected bounding box relative to the GNSS receiver are calculated. The distance between the GNSS receiver and the buildings can be obtained subsequently. Moreover, building height (which can be exemplarily extracted from Google Earth) is employed to extend the detected building height to the exact height.

Step II: The building boundaries are projected into a GNSS skyplot based on their azimuth angle, elevation angles relative to the GNSS receiver, and yaw angle provided by the INS.

Step III: Considering satellites' elevation angle, azimuth angle, SNR, and detected bounding box's information (elevation and azimuth angles in skyplot), satellites blocked by buildings are detected. Consequently, NLOS correction is implemented with an NLOS error model.

Step IV: Implementing GNSS WLS based on the corrected pseudorange measurements and healthy pseudorange measurements.

(2) Experimental Evaluation

The experiment evaluation is performed in an urban canyon with the same sensor setup as the one in Section III-A. Three GNSS positioning methods are compared to verify the proposed method:

- (1) WLS: GNSS positioning with the WLS.
- (2) WLS-NE: WLS with NLOS exclusion.
- (3) WLS-NC: WLS with proposed NLOS correction.

Fig. 7 and TABLE II show the comparison of positioning results between the conventional WLS and the proposed method. The GNSS positioning based on WLS with NLOS exclusion is also presented in TABLE II. As can be seen from Fig. 7, the total satellite numbers fluctuate between 5 and 13, with a mean satellite number of 10 during the experiment. With the aid of the proposed NLOS correction method, the positioning performance is improved at most of the epochs, which is indicated by the blue curve in the bottom panel of Fig. 7. 30.29 meters of mean positioning error and 19.86 meters of standard deviation were obtained using the WLS method without any NLOS exclusion or correction. After the NLOS exclusion (all the NLOS are excluded), the mean error goes up to 189.25 meters. The main reason for this dramatic increase is due to the distortion of satellites' geometric distribution. In other words, the HDOP increases significantly. According to the experiment, approximately 2~6 satellites are classified as NLOS due to the blockage from surrounding buildings. Therefore, the availability of GNSS positioning is decreased to only 75% due to the lack of satellites (at least five satellites are needed for GPS/BeiDou-based positioning calculation). The positioning error decreases to 22.86 meters using the proposed NLOS correction method. Moreover, the availability of GNSS positioning is also remained unchanged with the conventional WLS. This result shows that the proposed NLOS correction model can obtain improved GNSS

positioning performance.

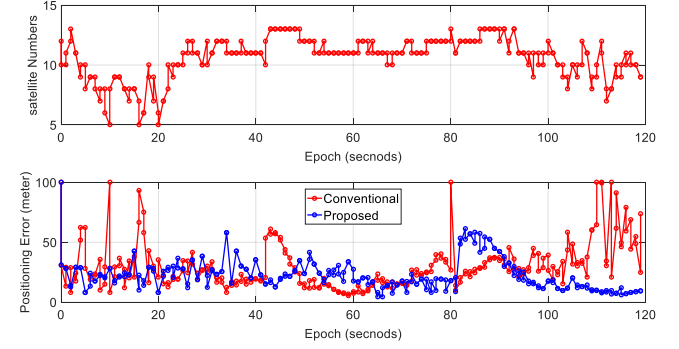


Fig. 7. Positioning error of the GNSS before and after adding the NLOS correction in an urban canyon. The top panel indicates the satellite numbers. The bottom panel shows the positioning error: the red curve indicates the positioning error using WLS, the blue curve denotes the positioning based on proposed NLOS correction [10].

TABLE II. POSITIONING PERFORMANCE OF THE TWO METHODS IN MIDDLE URBAN SCENARIO (IN THE UNIT OF METER) [10]

All data	WLS	WLS-NE	WLS-NC
Mean error	30.29	189.25	22.86
Std	19.86	71.01	13.17
Availability	100%	75%	100%

C. GNSS/LiDAR Integration Aided by Object Detection

(1) Methodology

NLOS correction method aided by LiDAR perception in Section III-B relaxes the drawback of excessive NLOS exclusion. However, the performance of NLOS correction relies heavily on the performance of the detection of reflecting point of the NLOS signals. The accuracy of NLOS detection in [10] can be significantly degraded in complex urban canyons. In this section, a generalized solution to cope with the detected NLOS receptions is presented based on the work in [32], where the uncertainty of NLOS is re-modeled. The GNSS/LiDAR integration is performed to show the feasibility of GNSS NLOS remodeling in sensor fusion. The flowchart of the GNSS/LiDAR integration solution is shown in Fig. 8.

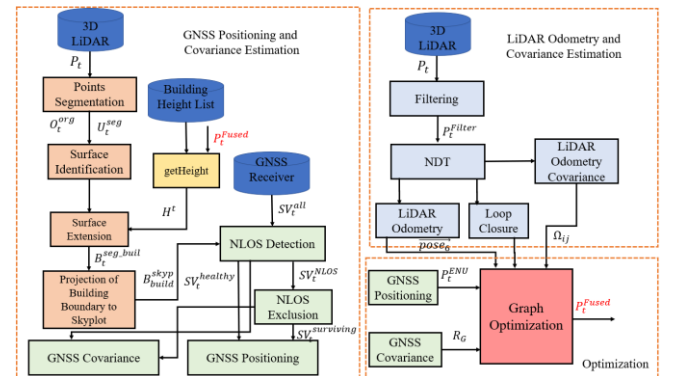


Fig. 8. The flowchart of the proposed GNSS/LiDAR integration method. Three parts are included: (a). GNSS positioning and its adaptive covariance estimation, (b). LiDAR odometry and its covariance estimation and (c). The graph-based optimization [32].

Firstly, the building boundary is detected based on the algorithm proposed in the previous work [33] of our research team. The point clouds are fixed to the GNSS frame based on the orientation obtained from LiDAR odometry (shown in Fig. 8). The satellites and the building boundary are both projected to a GNSS skyplot. Secondly, the NLOS detection is conducted based on a proposed NLOS detection algorithm. GNSS measurements suffered from both NLOS, and low elevation angle is excluded based on a proposed fault detection and exclusion (FDE) algorithm. Then, the GNSS positioning is conducted based on the survived GNSS measurements. Thirdly, the GNSS positioning covariance is calculated by considering the potential positioning errors caused by NLOS receptions. Finally, the improved GNSS positioning result and corresponding covariance are integrated with the LiDAR odometry using a graph-based SLAM framework.

(2) Experimental Evaluation

The experiment evaluation is performed in an urban canyon with the same sensor setup as the one in Section III-A. The GNSS standalone positioning is firstly presented. Then, the evaluation of GNSS/LiDAR integration is presented subsequently. GNSS positioning is evaluated by comparing the three methods:

- (1) **WLS** [3]: The WLS-based GNSS positioning.
- (2) **WLS-NE-A** [32]: The WLS-based GNSS positioning with all the GNSS NLOS receptions being excluded.
- (3) **WLS-NE-P** [32]: The WLS-based GNSS positioning with only part of the GNSS NLOS receptions being excluded.

The result of the horizontal GNSS positioning using different methods is listed in TABLE III. The conventional WLS method can obtain 29.81 meters of mean error. The error magnitude is much larger than the positioning error in [34] where its experiment is conducted in less urbanized areas. The standard deviation is 21.09 and the availability is 100% during the test. With the exclusion of all the NLOS measurements, the GNSS positioning is even worse. The mean of its positioning error goes up to 30.25 meters and the standard deviation also slightly increases. This result shows that the exclusion of all NLOS measurements may not improve the overall performance in highly urbanized areas. This is due to the distortion of the satellite's geometric distribution, namely, a larger HDOP occurs.

TABLE III
PERFORMANCE OF THE THREE GNSS POSITIONING METHODS (2D POSITIONING) [32]

All data	Conventional: WLS	WLS-NE-A	WLS-NE-P
Mean Error	29.81 m	30.25 m	27.09 m
std	21.09 m	22.28 m	19.6 m
Availability	100%	97.45%	100%

With the help of the proposed method, the mean positioning error is only slightly improved from 29.81 to 27.09 meters. The improvement is not dramatic because of

the excessive NLOS receptions in the tested scenario. The trajectory of the tested vehicle is shown in Fig. 9. The red circles represent the GNSS positioning results using the proposed WLS-NE method. The green curve indicates the ground truth of the tested trajectory. We can see from the figure that the majority of the epochs possess large positioning errors.



Fig. 9. The trajectory of the autonomous vehicle is indicated by the green curve. The red circles indicate the GNSS positioning result [32].

To verify the effectiveness of the proposed method in GNSS/LiDAR integration, three GNSS/LiDAR integration methods are compared.

- **Method (a):** GNSS/LiDAR integration with conventional GNSS covariance estimation [35].
- **Method (b):** GNSS/LiDAR integration with proposed GNSS covariance estimation.
- **Method (c):** GNSS/LiDAR integration with proposed GNSS covariance estimation. However, GNSS positioning is integrated into the graph optimization only when the adaptive covariance is smaller than a pre-determined threshold.

The GNSS/LiDAR integration results are given in Table IV using the listed three methods. The mean error of the conventional GNSS/LiDAR integration is 24.07 meters and is improved comparing with the performance of the GNSS standalone (27.09 meters). With the aid of proposed GNSS positioning covariance (Method (b)), the error of GNSS/LiDAR integration is slightly decreased to 22.67 meters. The standard deviation is also slightly decreased. In the integration method (b), all the GNSS positioning results and corresponding covariance are applied in the GNSS/LiDAR integration. As the majority of the GNSS positioning is erroneous, it is reasonable to use GNSS results only when it is accurate. Decent improvement is obtained after the constraint of covariance is applied. The mean error and standard deviation are decreased to 12.67 and 6.57 meters, respectively. This improvement shows that the proposed

covariance estimation can improve the performance of the GNSS/LiDAR integration. Comparing to the Bayes filter-based [36, 37] sensor fusion method, the graph-based GNSS/LiDAR integration takes all the constraints into the optimization framework. Thus, the poses of the whole organized point clouds, nodes, edges changed over time.

TABLE IV
EXPERIMENT 2: PERFORMANCE OF THE THREE GNSS/LIDAR INTEGRATION METHODS [32]

All data	Method (a)	Method (b)	Method (c)
Mean Error	25.68 m	8.14 m	7.49 m
STD	28.09 m	6.73 m	5.43 m
Availability	100%	100%	100%

IV. CAMERA/LIDAR AIDED GNSS POSITIONING WITH NLOS CORRECTION

The results in Section III show the effectiveness of the LiDAR perception aided GNSS positioning. In fact, the LiDAR sensor mainly plays two roles in Section III: 1) detect the dynamic objects [29] or surrounding buildings [10] for further NLOS detection. 2) measure the distance between the GNSS receiver and the reflecting point [10] for NLOS correction. Therefore, both the methods [10, 29] relies heavily on the LiDAR-based object detection. However, the performance of LiDAR-based perception can be significantly challenged in high dynamic environments. Recently, the camera [38-40] is adopted to capture the sky view image and satellite visibility is classified by segmenting the sky view. Improved performance is obtained by excluding the detected NLOS receptions. However, the fully NLOS exclusion shares the same drawbacks with the work in [29] where the geometry of the satellite distribution can be severely distorted. As a result, the GNSS positioning can even be degraded, due to the improper NLOS exclusion.

(1) Methodology

This section explores to make use of the camera to detect the NLOS receptions and 3D LiDAR to correct the NLOS receptions in urban canyon based on our work in [41]. The flowchart of the proposed method is given in Fig .10. The GNSS raw measurements, including satellite elevation and azimuth angles, pseudorange measurements, are obtained from the receiver. The sky view image is collected using a sky-pointing fish-eye camera with a field of view of -90 to +90 degrees vertically. The satellites are then projected into the segmented image with the aid of the heading angle from AHRS. The LOS/NLOS measurements can be classified using the perceived and segmented sky view image. The 3D LiDAR provides the point clouds of the surrounding. Therefore, the distance from the GNSS receiver to the surroundings can be obtained from the raw point clouds. The NLOS correction is then estimated using a deterministic NLOS model [9]. Finally, the GNSS SPP is conducted using WLS.

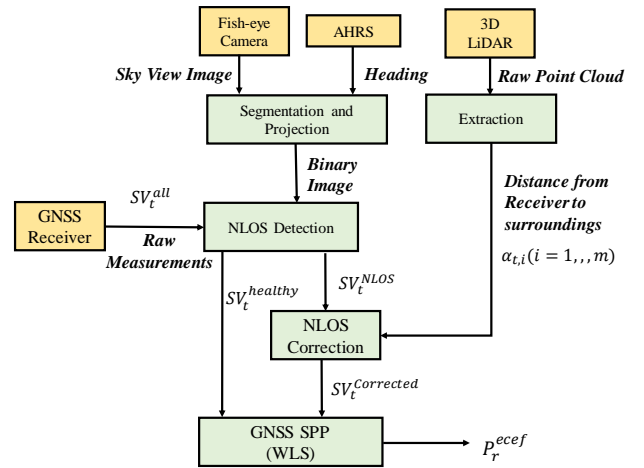


Fig. 10. Overview of the proposed algorithm of the camera/LiDAR aided GNSS positioning with nlos correction. The main inputs are GNSS raw measurements, sky view image from fish-eye camera and real-time 3D point clouds from 3D LiDAR. The auxiliary input is the heading angle from INS or AHRS [41].

(2) Experimental Evaluation

During the experiment, a u-blox M8T GNSS receiver was used to collect raw GPS/BeiDou measurements at a frequency of 1 Hz. The sky-pointing fisheye camera was employed to capture the sky view image at a frequency of 10 Hz. The Xsens Ti-10 IMU (which can also act as AHRS) was employed to collect data at a frequency of 100 Hz to provide the heading angle for the fish-eye camera. In addition, the NovAtel SPAN-CPT was also used to provide the ground truth. All the data were collected and synchronized under the robot operation system (ROS) [42]. The coordinate systems between all the sensors were calibrated before the experiments.

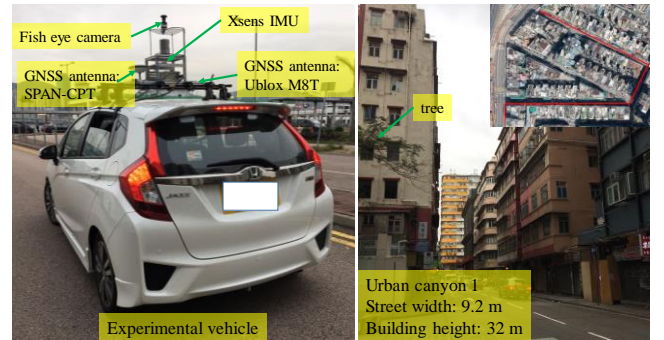


Fig. 11. Experimental vehicle and sensor setup in the left-hand side figure. Tested scenarios of urban canyon [41].

To verify the effectiveness of the proposed method, three GNSS positioning methods are compared:

- **WLS:** Weighted least square [43].
- **WLS-NE:** WLS + NLOS exclusion (WLS-NE): excluding the NLOS measurements detected using a fisheye camera and perform WLS.
- **WLS-NC:** WLS + NLOS correction (WLS-NC): correcting the NLOS measurements detected using a fisheye camera and perform WLS.

The GNSS positioning performance of the listed three methods is shown in Table V. 27.18 meters of mean positioning error is obtained using the conventional WLS method with the maximum error reaching 131.81 meters. After all the NLOS satellites detected using the fish-eye camera being excluded from WLS calculation, the positioning error increases to more than 58 meters. Moreover, the standard deviation also increases from 22.28 meters to 86.13 meters. Due to the excessive NLOS exclusion, the availability of GNSS positioning decreases from 100% to 9.70%. With the help of the proposed NLOS detection and correction method, the GNSS positioning error decreases to 18.49 meters and the standard deviation also decreases slightly compared with the WLS. The improved GNSS positioning performance shows the effectiveness of the proposed method. Moreover, the availability of the proposed method is also guaranteed using the proposed method. The LOS/NLOS satellite numbers are shown in Table VI. The mean numbers of LOS and NLOS satellites are 2.89 and 8.08, respectively. During the experiments, the NLOS satellites make up 73.65% of all the satellites due to the blockage from the surrounding tall buildings. Interestingly, at least 2 satellites are NLOS during the experiment and the maximum number of NLOS satellites reaches 14.

The satellite distributions inside the sky view image in several epochs are shown in Fig. 12. The red circle shows the NLOS satellite and the blue circle shows the healthy satellite. The numbers inside the Figures show the accuracy of WLS and WLS-NC, respectively. As the satellite classification accuracy relies on the performance of the image processing [41], some of the NLOS satellites can be misclassified due to the illumination sensitivity of the image processing algorithm. For example, the satellites near the building boundaries are misclassified shown in Fig. 12-(A) and Fig. 12-(I).

TABLE V
PERFORMANCE OF THE GNSS SPSS IN URBAN CANYON [41]

GNSS Positioning	WLS	WLS-NE	WLS-NC
Mean error	27.18 m	58.57 m	18.49 m
Std	22.28 m	86.13 m	15.27 m
Maximum error	131.81 m	156.29 m	73.37 m
Availability	100%	9.70%	100%

TABLE VI
SATELLITE NUMBERS IN URBAN CANYON [41]

Satellite	LOS	NLOS	LOS&NLOS
Mean number	2.89	8.08	10.97
Std	1.75	2.54	2.49
Max number	12	14	16
Min number	0	2	5
Percentage	26.34%	73.65%	

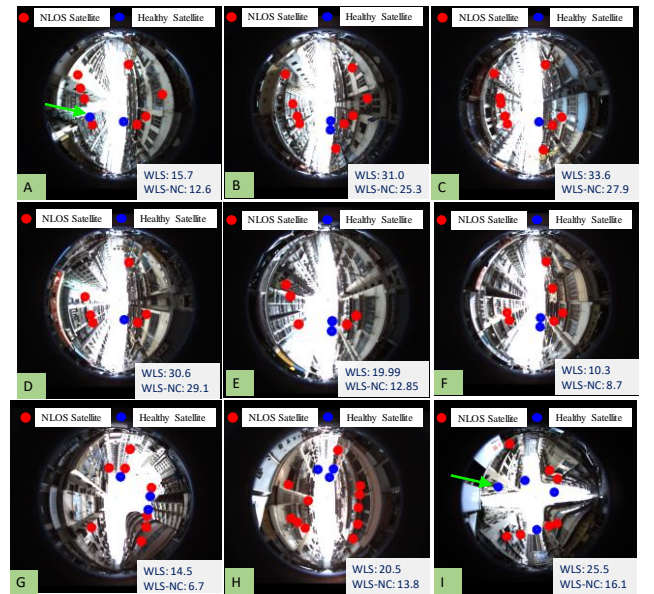


Fig. 12. Illustration of Skyplot which indicates the satellite distribution during the dynamic experiment. The green circle represents the satellites that are healthy. The red circle denotes the NLOS satellites [41].

V. CONCLUSIONS AND FUTURE WORK

Achieving robust and accurate positioning in urban canyons with numerous dynamic objects and high-rising buildings is still a challenging problem. Effectively perceiving the surrounding environment is effective for figuring out the potential sources of error. With the fast development of the capability of perception, partially or even fully describing the surrounding environments based on onboard sensors becomes possible. This paper proposes a novel sensor integration scheme, the PASIN, which leverages the perception to assist the single sensor measurements before its integration with other sensors. Several applications are presented in this paper to verify the effectiveness of the proposed PASIN. We believe that the proposed method can have a positive impact on both the academic and industrial fields. In future work, we will make use of the online perception to mitigate the effects of dynamic objects on the other sensors, such as camera and 3D LiDAR. In addition, we will explore to identify the context of the environment using the online perception to assist onboard sensors.

ACKNOWLEDGMENT

The authors acknowledge the support of the Hong Kong PolyU internal grant on the project ZVKZ, "Navigation for Autonomous Driving Vehicle using Sensor Integration".

REFERENCES

- [1] A. Geiger, P. Lenz, and R. Urtasun, "Are we ready for autonomous driving? the kitti vision benchmark suite," in *2012 IEEE Conference on Computer Vision and Pattern Recognition*, 2012: IEEE, pp. 3354-3361.
- [2] G. Wan, X. Yang, R. Cai, H. Li, H. Wang, and S. Song, "Robust and Precise Vehicle Localization based on Multi-sensor Fusion in Diverse City Scenes," *arXiv preprint arXiv:1711.05805*, 2017.
- [3] P. D. Groves, *Principles of GNSS, inertial, and multisensor integrated navigation systems*. Artech house, 2013.

- [4] W. Wen *et al.*, "UrbanLoco: A Full Sensor Suite Dataset for Mapping and Localization in Urban Scenes," 2019.
- [5] W. Z. Weisong Wen, Li-ta Hsu, "Robust Localization Using 3D NDT Matching and Beam Model for Autonomous Vehicles in an Urban Scenario with Dynamic Obstacles," in *The 11th International Conference on Mobile Mapping Technology (MMT 2019)*, Shenzhen, China, 2019.
- [6] W. Wen, X. Bai, Y.-C. Kan, and L.-T. Hsu, "Tightly Coupled GNSS/INS Integration Via Factor Graph and Aided by Fish-eye Camera," *Ieee T Veh Technol*, 2019.
- [7] W. Wen, G. Zhang, and L.-T. Hsu, "Exclusion of GNSS NLOS receptions caused by dynamic objects in heavy traffic urban scenarios using real-time 3D point cloud: An approach without 3D maps," in *Position, Location and Navigation Symposium (PLANS), 2018 IEEE/ION*, 2018: IEEE, pp. 158-165.
- [8] W. W. Xiwei Bai, Li-Ta Hsu, "Performance Analysis of Visual/Inertial Integrated Positioning in Typical Urban Scenarios of Hong Kong," in *Proceedings of 2019 Asian-Pacific Conference on Aerospace Technology and Science* Taiwan, 2019.
- [9] L.-T. Hsu, "Analysis and modeling GPS NLOS effect in highly urbanized area," *GPS Solutions*, journal article vol. 22, no. 1, p. 7, November 04 2018, doi: 10.1007/s10291-017-0667-9.
- [10] W. Wen, G. Zhang, and L. T. Hsu, "Correcting NLOS by 3D LiDAR and building height to improve GNSS single point positioning," *Navigation*, vol. 66, no. 4, pp. 705-718, 2019.
- [11] P. D. Groves and M. Adjrak, "Likelihood-based GNSS positioning using LOS/NLOS predictions from 3D mapping and pseudoranges," *Gps Solut*, vol. 21, no. 4, pp. 1805-1816, 2017.
- [12] W. Wen, X. Bai, W. Zhan, M. Tomizuka, and L.-T. Hsu, "Uncertainty estimation of LiDAR matching aided by dynamic vehicle detection and high definition map," *Electronics letters*, 2019.
- [13] W. Wen, L.-T. Hsu, and G. Zhang, "Performance Analysis of NDT-based Graph SLAM for Autonomous Vehicle in Diverse Typical Driving Scenarios of Hong Kong," *Sensors*, vol. 18, no. 11, p. 3928, 2018. [Online]. Available: <http://www.mdpi.com/1424-8220/18/11/3928>.
- [14] T. D. Barfoot, *State Estimation for Robotics*. Cambridge University Press, 2017.
- [15] Y. C. K. Weisong Wen, Li-Ta Hsu, "Performance Comparison of GNSS/INS Integrations Based on EKF and Factor Graph Optimization," presented at the ION GNSS+ 2019, Florida, 2019.
- [16] M. Kaess, H. Johannsson, R. Roberts, V. Ila, J. J. Leonard, and F. Dellaert, "iSAM2: Incremental smoothing and mapping using the Bayes tree," *The International Journal of Robotics Research*, vol. 31, no. 2, pp. 216-235, 2012.
- [17] S. Thrun, W. Burgard, and D. Fox, *Probabilistic robotics*. MIT press, 2005.
- [18] F. Dellaert and M. Kaess, "Factor graphs for robot perception," *Foundations and Trends® in Robotics*, vol. 6, no. 1-2, pp. 1-139, 2017.
- [19] T. Qin, P. Li, and S. Shen, "Vins-mono: A robust and versatile monocular visual-inertial state estimator," *IEEE Transactions on Robotics*, vol. 34, no. 4, pp. 1004-1020, 2018.
- [20] V. Indelman, S. Williams, M. Kaess, and F. Dellaert, "Factor graph based incremental smoothing in inertial navigation systems," in *Information Fusion (FUSION), 2012 15th International Conference on*, 2012: IEEE, pp. 2154-2161.
- [21] S. Lange, N. Sünderhauf, and P. Protzel, "Incremental smoothing vs. filtering for sensor fusion on an indoor UAV," in *Robotics and Automation (ICRA), 2013 IEEE International Conference on*, 2013: IEEE, pp. 1773-1778.
- [22] W. Li, X. Cui, and M. Lu, "A robust graph optimization realization of tightly coupled GNSS/INS integrated navigation system for urban vehicles," *Tsinghua Science and Technology*, vol. 23, no. 6, pp. 724-732, 2018.
- [23] N. Sünderhauf and P. Protzel, "Switchable constraints for robust pose graph SLAM," in *2012 IEEE/RSJ International Conference on Intelligent Robots and Systems*, 2012: IEEE, pp. 1879-1884.
- [24] T. Pfeifer, S. Lange, and P. Protzel, "Dynamic Covariance Estimation—A parameter free approach to robust Sensor Fusion," in *2017 IEEE International Conference on Multisensor Fusion and Integration for Intelligent Systems (MFI)*, 2017: IEEE, pp. 359-365.
- [25] T. Pfeifer and P. Protzel, "Expectation-maximization for adaptive mixture models in graph optimization," in *2019 International Conference on Robotics and Automation (ICRA)*, 2019: IEEE, pp. 3151-3157.
- [26] R. M. Watson, J. N. Gross, C. N. Taylor, and R. C. Leishman, "Uncertainty Model Estimation in an Augmented Data Space for Robust State Estimation," *arXiv preprint arXiv:1908.04372*, 2019.
- [27] T. Pfeifer and P. Protzel, "Incrementally learned Mixture Models for GNSS Localization," *arXiv preprint arXiv:1904.13279*, 2019.
- [28] Y. Sun, M. Liu, and M. Q.-H. Meng, "Improving RGB-D SLAM in dynamic environments: A motion removal approach," *Robotics and Autonomous Systems*, vol. 89, pp. 110-122, 2017.
- [29] W. Wen, G. Zhang, and L.-T. Hsu, "GNSS NLOS Exclusion Based on Dynamic Object Detection Using LiDAR Point Cloud," *Ieee T Intell Transp*, 2019.
- [30] G. Z. Weisong Wen, Li-ta Hsu, "Correcting GNSS NLOS by 3D LiDAR and Building Height," presented at the ION GNSS+, 2018, Miami, Florida, USA., 2018.
- [31] J. Marshall, "Creating and viewing skyplots," *Gps Solut*, vol. 6, no. 1-2, pp. 118-120, 2002.
- [32] Z. G. Wen W., Hsu, L.T, "Object Detection Aided GNSS and Its Integration with LiDAR in Highly Urbanized Areas,," *IEEE Intelligent Transportation Systems Magazine (accepted)*, p. Accepted, 2019.
- [33] W. Wen, G. Zhang, and L.-T. Hsu, "Exclusion of GNSS NLOS Receptions Caused by Dynamic Objects in Heavy Traffic Urban Scenarios Using Real-Time 3D Point Cloud: An Approach without 3D Maps," *arXiv preprint arXiv:1804.10917*, 2018.
- [34] S. Peyraud *et al.*, "About Non-Line-Of-Sight Satellite Detection and Exclusion in a 3D Map-Aided Localization Algorithm," *Sensors*, vol. 13, no. 1, pp. 829-847, 2013. [Online]. Available: <http://www.mdpi.com/1424-8220/13/1/829>.
- [35] D. Maier and A. Kleiner, "Improved GPS sensor model for mobile robots in urban terrain," in *Robotics and Automation (ICRA), 2010 IEEE International Conference on*, 2010: IEEE, pp. 4385-4390.
- [36] G. P. Huang, A. I. Mourikis, and S. I. Roumeliotis, "Analysis and improvement of the consistency of extended Kalman filter based SLAM," in *Robotics and Automation, 2008. ICRA 2008. IEEE International Conference on*, 2008: IEEE, pp. 473-479.
- [37] J. Zhu, N. Zheng, Z. Yuan, Q. Zhang, X. Zhang, and Y. He, "A SLAM algorithm based on the central difference Kalman filter," in *Intelligent Vehicles Symposium, 2009 IEEE*, 2009: IEEE, pp. 123-128.
- [38] J. I. Meguro, T. Murata, J. I. Takiguchi, Y. Amano, and T. Hashizume, "GPS multipath mitigation for urban area using omnidirectional infrared camera," *Ieee T Intell Transp*, vol. 10, no. 1, pp. 22-30, 2009.
- [39] T. Suzuki, M. Kitamura, Y. Amano, and T. Hashizume, "High-accuracy GPS and GLONASS positioning by multipath mitigation using omnidirectional infrared camera," in *IEEE International Conference on Robotics and Automation*, 2011, pp. 311-316.
- [40] J. S. Sánchez, A. Gerhmann, P. Thevenon, P. Brocard, A. B. Afia, and O. Julien, "Use of a FishEye camera for GNSS NLOS exclusion and characterization in urban environments," in *ION ITM 2016, International Technical Meeting*, 2016: ION.
- [41] W. W. Xiwei Bai, Li-Ta Hsu, "Using Sky-Pointing Fish-eye Camera and LiDAR to Aid GNSS Single Point Positioning in Urban Canyons (submitted)," *IET Intelligent Transport Systems*, 2019.
- [42] M. Quigley *et al.*, "ROS: an open-source Robot Operating System," in *ICRA workshop on open source software*, 2009, vol. 3, no. 3.2: Kobe, Japan, p. 5.
- [43] A. M. Herrera, H. F. Suhandri, E. Realini, M. Reguzzoni, and M. C. de Lacy, "goGPS: open-source MATLAB software," *Gps Solut*, vol. 20, no. 3, pp. 595-603, 2016.